SPECIAL TOPIC — Acoustics

Selective generation of ultrasonic Lamb waves by electromagnetic acoustic transducers*

Ming-Liang Li(李明亮), Ming-Xi Deng(邓明晰)†, and Guang-Jian Gao(高广健)

Department of Physics, Logistics Engineering University, Chongqing 401331, *China*

(Received 14 March 2016; revised manuscript received 27 June 2016; published online 25 October 2016)

In this paper, we describe a modal expansion approach for the analysis of the selective generation of ultrasonic Lamb waves by electromagnetic acoustic transducers (EMATs). With the modal expansion approach for waveguide excitation, an analytical expression of the Lamb wave's mode expansion coefficient is deduced, which is related to the driving frequency and the geometrical parameters of the EMAT's meander coil, and lays a theoretical foundation for exactly analyzing the selective generation of Lamb waves with EMATs. The influences of the driving frequency on the mode expansion coefficient of ultrasonic Lamb waves are analyzed when the EMAT's geometrical parameters are given. The numerical simulations and experimental examinations show that the ultrasonic Lamb wave modes can be effectively regulated (strengthened or restrained) by choosing an appropriate driving frequency of EMAT, with the geometrical parameters given. This result provides a theoretical and experimental basis for selectively generating a single and pure Lamb wave mode with EMATs.

Keywords: ultrasonic Lamb waves, selective generation, electromagnetic acoustic transducer (EMAT), Lorentz surface stress

PACS: 43.20.–f, 43.35.–c **DOI:** 10.1088/1674-1056/25/12/124301

1. Introduction

An electromagnetic acoustic transducer (EMAT) can be effectively used for the non-contact nondestructive testing and evaluating (NDT & E) of metallic material/structure. The main advantage of the inspection technique using EMATs over that using piezoelectric transducers is that no couplant is required.[1–3] As is well known, the ultrasonic Lamb wave technique can be widely used in NDT & E of the plate-like structure.[4–6] Recently, investigations on the generation and detection of ultrasonic Lamb waves with EMAT have received considerable attention. Dhayalan and Balasubramaniam used a finite element model and a time-frequency analysis to simulate the generations of Lamb wave modes with a meander-coil EMAT, and to analyze the interaction of Lamb wave modes with defects.[7] Masahiko and Hirotsugu systematically analyzed the EMAT's physical principle and its detection technology.[8] Rueter and Morgenstern investigated the EMAT concepts including only the coil and generated ultrasound with high pulsed power.[9] Zhai *et al.* proposed an approach to removing the effect of multiple wavelengths by changing the geometric pattern of the EMAT's meander coils.[10]

As is well known, ultrasonic Lamb waves generated by meander-coil EMATs generally include multi-modes,[11] which will hinder the application of the EMAT inspection technique that often requires the selective generation of a single and pure Lamb wave mode. Therefore, it is of important significance to find an approach to controlling or regulating the generations of Lamb wave modes by appropriately choosing the geometrical parameters of the EMAT's meander coil and/or the driving frequency. In previous work, the influences of the EMAT's geometrical parameters on the generation of ultrasonic Lamb waves were investigated.[12] It is found that at a given driving frequency, a single and pure Lamb wave mode can be effectively generated with the meander-coil EMAT through appropriately changing its geometrical parameters. However, in practical applications, changing the driving frequency is more convenient than changing the EMAT's geometrical parameters. Based on the analytical expression of the Lamb wave's mode expansion coefficient that is closely related to the driving frequency and the EMAT's geometrical parameters, this paper focuses on investigating the selective generations of Lamb wave modes at different driving frequencies of EMAT when its geometrical parameters are set. Theoretical analyses and experimental results show that a single and pure Lamb wave mode can be selectively generated at some appropriate driving frequencies. This result is of practical significance for the non-contact NDT & E of metallic materials/structures using the EMAT inspection technique.

2. Theoretical fundamentals

When the EMAT technique is used to inspect a ferromagnetic material/structure, the mechanisms both of the Lorentz force and the magnetostrictive effect must be taken into account simultaneously.[8] However, the basic mechanism of the magnetostrictive effect is rather complicated, and

*Project supported by the National Natural Science Foundation of China (Grant Nos. 11474361 and 11274388).

†Corresponding author. E-mail: dengmx65@yahoo.com

© 2016 Chinese Physical Society and IOP Publishing Ltd

so far little work on it has been conducted. For simplicity, the material/structure to be inspected is assumed to be non-ferromagnetic, and only the mechanism of the Lorentz force needs to be considered.

The two-dimensional model of a meander-coil EMAT for generating Lamb waves in a non-ferromagnetic plate (aluminum sheet) with a thickness of $2d$ is shown in Fig. 1, where the oz- and oy-axis directions, respectively, indicate the direction of the Lamb wave propagation and that of the sheet thickness. The parameter a is the width of the single wire of the meander coil, and D and L are, respectively, the spatial period and total length of the meander coil. The lift-off distance of the coil (denoted by g) is assumed to be unchanged throughout the whole analyses. The uniform static bias magnetic field $\boldsymbol{B}_{\rm s}$ produced by a permanent magnet is applied to the meander coil, and typically its width is slightly larger than the total length L of the meander coil.

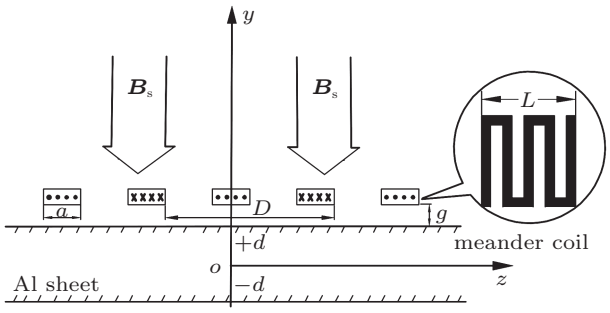


Fig. 1. Two-dimensional model of an EMAT for selectively generating Lamb waves.

An alternating current $i(t) = I\exp(\mathrm{j}\omega t)$ with the driving frequency f (angular frequency $\omega = 2\pi f$) is applied to the meander coil (see Fig. 1). For simplicity, it is assumed that the current within the single wire is uniformly distributed. Thus the dynamic magnetic field $\boldsymbol{H}^{\rm V}$ beneath the meander coil will be induced by the alternating current $i(t)$. Further, based on the boundary condition of the magnetic field that passes through the surface of the material, the dynamic magnetic field $\boldsymbol{H}^{\rm M}$ in the sheet can also be determined.[8,12] It is known that the dynamic magnetic field $\boldsymbol{H}^{\rm M}$ in the aluminum sheet decreases exponentially along the sheet thickness due to the electromagnetic skin effect. So it can be regarded as the dynamic magnetic field in the aluminum sheet existing only within the electromagnetic skin depth δ beneath the upper surface $y = +d$ (see Fig. 1).[12]

The previous studies have shown that the electric eddy current J_e induced by the dynamic magnetic field $\boldsymbol{H}^{\rm M}$ (within the electromagnetic skin depth δ) generated by the alternating current $i(t)$ in the meander coil is along the ox-axis direction, and the magnitude of its density can approximately be given by:[8,12]

$$J_e = \frac{\partial H_z^{\rm M}}{\partial y}, \tag{1}$$

where $H_z^{\rm M}$ denotes the oz-axis component of the dynamic magnetic field $\boldsymbol{H}^{\rm M}$ in the aluminum sheet, generated by the meander coil, and its mathematical expression has been presented in Ref. [12].

Generally, both the static magnetic field $\boldsymbol{B}_{\rm s}$ and the dynamic magnetic field $\boldsymbol{H}^{\rm M}$ will contribute to the Lorentz force occurring in the solid sheet. It is known that the magnitude of $\boldsymbol{H}^{\rm M}$ is far less than that of $\boldsymbol{B}_{\rm s}$ when the magnitude of the driving alternating current $i(t)$ is relatively small.[8] For simplicity, only the static magnetic field will be considered in the subsequent analyses. Herein, the mathematical expression of the Lorentz force can be given by[8,12]

$$\boldsymbol{F}_{\rm L} = -\boldsymbol{B}_{\rm s} \times \frac{\partial H_z^{\rm M}}{\partial y}\hat{x}, \tag{2}$$

where $\hat{x}$ is the unit vector along the ox axis.

As is well known, the Lorentz force $\boldsymbol{F}_{\rm L}$ generated by the eddy current is a body force only with the oz-axis component, and both the eddy current and the Lorentz force exist in the same depth (mainly within the electromagnetic skin depth δ).[12] Generally, the skin depth δ is far less than the acoustic wavelength at the same frequency.[8] Thus, the Lorentz force occurring within the electromagnetic skin depth δ can approximately be regarded as a shear stress P_{zy} exerted on the sheet surface $y = +d$ in Fig. 1 (called the Lorentz surface stress), and it can formally be written as $P_{zy} = \int_{d-\delta}^{d} (\boldsymbol{F}_{\rm L} \cdot \hat{z})\,{\rm d}y$,[12] where $\hat{z}$ is the unit vector along the oz axis.

It is assumed that the Lorentz surface stress P_{zy} becomes zero outside the EMAT coverage $[z \in (-L/2, L/2)]$. According to the modal analysis approach for waveguide excitation,[12–14] the Lorentz surface stress P_{zy} can be regarded as an excitation source for the generation of a series of Lamb wave modes. In other words, the acoustic fields [including the fields of the mechanical displacement $\boldsymbol{U}(y,z)$, velocity $\boldsymbol{v}(y,z)$ and stress tensor $\boldsymbol{P}(y,z)$], generated by the Lorentz surface stress $P_{zy} = P_{zy}(z)[z \in (-L/2, L/2)]$, can be regarded as the sum of a series of Lamb wave modes, namely[12,14]

$$\begin{cases} \boldsymbol{U}(y,z) = \sum\limits_n a_n(z)\boldsymbol{U}_n(y), \\ \boldsymbol{v}(y,z) = \sum\limits_n a_n(z)\boldsymbol{v}_n(y), \\ \boldsymbol{P}(y,z)\cdot\hat{z} = \sum\limits_n a_n(z)\boldsymbol{P}_n(y)\cdot\hat{z}, \end{cases} \tag{3}$$

where $a_n(z)$ is the mode expansion coefficient of the n-th Lamb wave, and $\boldsymbol{U}_n(y)$, $\boldsymbol{v}_n(y)$, and $\boldsymbol{P}_n(y)$ are the corresponding fields of the mechanical displacement, velocity, and stress, respectively. The equation governing the Lamb wave's expansion coefficient $a_n(z)$ takes the following form:[12–14]

$$\left(\frac{\partial}{\partial z} - \mathrm{j}k_n\right) a_n(z) = \frac{f_{sn}(z)}{4P_{nn}}, \tag{4}$$

where the surface excitation source $f_{sn}(z)$ caused by the Lorentz force within the skin depth is given by

$$f_{sn}(z) = [\hat{z}\cdot\tilde{\boldsymbol{v}}_n(y)]\cdot P_{zy}(z)|_{y=+d}, z \in (-L/2, L/2). \tag{5}$$

In Eq. (5) and the subsequent mathematical equations, the superscript "$\sim$" denotes the complex conjugate of the corresponding physical quantity. P_{nn} is the average flow power (per unit length along the ox axis) of the n-th Lamb wave mode (with the wave-number k_n), and it takes the following form:[12–14]

$$P_{nn} = \frac{1}{2}\mathrm{Re}\int_{-d}^{+d}\left\{\left[-\frac{\tilde{\partial}}{\partial t}\boldsymbol{U}_n(y)\cdot\boldsymbol{P}_n(y)\right]\cdot\hat{z}\right\}\mathrm{d}y. \tag{6}$$

Integration of Eq. (4) yields,[12]

$$\begin{aligned} a_n(z) &= \frac{1}{4P_{nn}}[\hat{z}\cdot\tilde{\boldsymbol{v}}_n(y)]|_{y=+d}\cdot\exp(\mathrm{j}k_n z) \\ &\quad\times\int P_{zy}(\zeta)\exp(-\mathrm{j}k_n\zeta)\mathrm{d}\zeta. \end{aligned} \tag{7}$$

Considering the fact that the Lorentz surface stress $P_{zy}(z)$ exists only in the EMAT coverage [namely $z\in(-L/2,L/2)$], equation (7) can be further written as[12]

$$\begin{aligned} a_n(z) &= \frac{1}{4P_{nn}}[\hat{z}\cdot\tilde{\boldsymbol{v}}_n(y)]|_{y=+d}\cdot\exp(\mathrm{j}k_n z) \\ &\quad\times\int_{-L/2}^{L/2}P_{zy}(\zeta)\exp(-\mathrm{j}k_n\zeta)\mathrm{d}\zeta \\ &= \frac{1}{4P_{nn}}[\hat{z}\cdot\tilde{\boldsymbol{v}}_n(y)]|_{y=+d}\cdot\exp(\mathrm{j}k_n z) \\ &\quad\times\left\{\int_{-\infty}^{+\infty}P_{zy}(\zeta)\exp(-\mathrm{j}k\zeta)\mathrm{d}\zeta\right\}_{k=k_n} \\ &= \frac{\pi}{2P_{nn}}[\hat{z}\cdot\tilde{\boldsymbol{v}}_n(y)]|_{y=+d}\cdot P_{zy}^*(k_n)\cdot\exp(\mathrm{j}k_n z), \end{aligned} \tag{8}$$

where $P_{zy}^*(k_n)$ is the magnitude of the spatial Fourier transform on $P_{zy}(z)$ (under the condition of $k=k_n$), and is determined by[8,12]

$$\begin{aligned} P_{zy}^*(k) &= \frac{1}{2\pi}\int_{-\infty}^{+\infty}P_{zy}(z)\cdot\exp(-\mathrm{j}kz)\mathrm{d}z \\ &= \frac{1}{2\pi}\int_{-L/2}^{L/2}\int_{d-\delta}^{d}\left[\left(-\boldsymbol{B}_\mathrm{s}\times\frac{\partial H_z^\mathrm{M}}{\partial y}\hat{x}\right)\cdot\hat{z}\right] \\ &\quad\times\exp(-\mathrm{j}kz)\mathrm{d}y\mathrm{d}z. \end{aligned} \tag{9}$$

Based on the mathematical expression of H_z^M given in Ref. [12], equation (9) can be further written as[12]

$$\begin{aligned} &P_{zy}^*(k) \\ &= \frac{B_\mathrm{s}Ik}{2\pi a}\sum_m\frac{A_m}{k^2-\xi_m^2}[\exp(q_m\delta)-1]\exp[-\xi_m(g+d)] \\ &\quad\times\left[\cos\left(\frac{\xi_m L}{2}\right)\sin\left(\frac{kL}{2}\right)-\frac{\xi_m}{k}\sin\left(\frac{\xi_m L}{2}\right)\cos\left(\frac{kL}{2}\right)\right], \end{aligned} \tag{10}$$

where $A_m = 4\sin[(2m+1)\pi a/D]/[(2m+1)\pi]$, $\xi_m = 2\pi(2m+1)/D$, $\delta = \sqrt{2/\omega\eta\bar{\mu}_{zz}}$, and $q_m = \sqrt{(\bar{\mu}_{zz}/\bar{\mu}_{yy})\xi_m^2+2\mathrm{j}/\delta^2}$. Moreover, the condition $\mathrm{Re}(q_m)<0$ is required.[8] The parameters $\bar{\mu}_{rr}$ ($r=y,z$) and η are, respectively, the relative magnetic permittivity and the conductivity of the plate material. It has been found that the shape of the $P_{zy}^*(k)/B_\mathrm{s}I$ curve is completely determined by the EMAT's geometrical parameters.[12] The magnitude of the wave-number k corresponding to the peak in the main lobe of the $P_{zy}^*(k)/B_\mathrm{s}I$ curve is largely dependent on the space period D (approximately $k=2\pi/D$), but is still associated with parameters L and a. It is also known that the longer the total length L of the EMAT's coil, the narrower the main lobe of the $P_{zy}^*(k)/B_\mathrm{s}I$ curve will be.

When the EMAT's geometrical parameters and the product of B_s and I (i.e., $B_\mathrm{s}I$) are given, the magnitude and shape of the $P_{zy}^*(k)$ curve will be completely determined. For a specified mode such as the n-th Lamb wave, different driving frequencies will result in different values of wave-number k_n based on the Lamb wave dispersion curve. Thus, the magnitude of $P_{zy}^*(k_n)$ in Eq. (8) can also be adjusted by changing the driving frequency f even if the EMAT's geometrical parameters and the product $B_\mathrm{s}I$ are given. Thus, the expression of the Lamb wave's mode expansion coefficient $a_n(z)$, determined by Eqs. (8)–(10), is closely associated with the EMAT's geometrical parameters (a, D, L) and the driving frequency, when the coil lift-off distance g (see Fig. 1) and the product $B_\mathrm{s}I$ are given.

The displacement field of the n-th Lamb wave mode can formally be expressed as follows:

$$\boldsymbol{U}_n(y,z) = \left(\frac{\pi P_{zy}^*(k_n)}{2P_{nn}}[\hat{\boldsymbol{z}}\cdot\tilde{\boldsymbol{v}}_n(y)]|_{y=+d}\right)\boldsymbol{U}_n(y)\exp(\mathrm{j}k_n z). \tag{11}$$

Equation (11) shows that the displacement field of the n-th Lamb wave mode is proportional to the magnitude of the spatial Fourier transform on $P_{zy}(z)$ under $k=k_n$. Clearly, it is expected that the n-th Lamb wave mode can be selectively generated (strengthened or restrained) by choosing the appropriate EMAT's geometrical parameters (a, D, L) and/or the driving frequency f.

3. Numerical analyses

It is known from the analytical results presented in Section 2 that the ultrasonic Lamb wave modes generated by EMAT are closely related to the driving frequency and the EMAT's geometrical parameters. In previous work, the influences of the EMAT's geometrical parameters on generation of the ultrasonic Lamb wave have been investigated, with the driving frequency f kept unchanged.[12] It is found that the Lamb wave's mode expansion coefficient can be appropriately adjusted by changing the EMAT's geometrical parameters, and thus the unwanted Lamb wave modes can be effectively restrained. Here, we will focus on analyzing the influences of the driving frequency on the selective generation of ultrasonic Lamb wave by EMAT, with the geometrical parameters given.

In the numerical analyses, the aluminum sheet is 1.82-mm thick, and its longitudinal and transverse speeds are

6.350 mm/μs and 3.100 mm/μs, respectively. The EMAT's geometrical parameters are set to be $a = 0.5$ mm, $D = 3$ mm, $L = 20$ mm, and $g = 0.5$ mm.

3.1. Influence of the driving frequency on the Lorentz surface stress

When the EMAT's geometrical parameters are given, through Eq. (10), the curve of the spatial Fourier transform, denoted by $P^*_{zy}(k)$, of the Lorentz surface stress $P_{zy} = P_{zy}(z)$ exerted on the surface of the aluminum sheet ($y = +d$) is calculated and shown on the left side of Fig. 2. The dispersion curves (wave-number k versus f) of Lamb wave propagation in a 1.82-mm-thick aluminum sheet are simultaneously presented on the right side of Fig. 2. Both the $P^*_{zy}(k)$ curve and the Lamb wave dispersion curves have the same wave-number axis. Clearly, from the mapping means shown in Fig. 2, it is easy to determine directly the magnitude of $P^*_{zy}(k_n)$ that contributes to the generation of the n-th Lamb wave mode at a given driving frequency (see Eq. (11)).

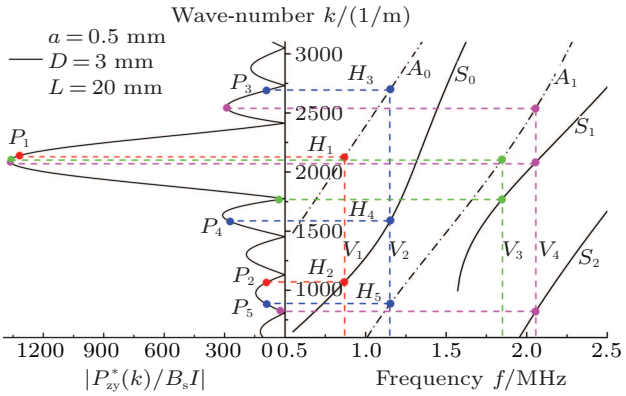


Fig. 2. (color online) Curves of the spatial Fourier transform of the Lorentz surface stress (left) and Lamb wave dispersion curves (right).

As an example, when the meander-coil EMAT (shown in Fig. 1) is driven at the frequency $f = 1.15$ MHz (given by the vertical dash line V_2 in Fig. 2), the Lamb wave modes A_0, S_0, and A_1 (determined by the intersections between the vertical dash line V_2 and the dispersion curves) may be generated. The corresponding magnitudes of $P^*_{zy}(k_n)$ that contribute to the generations of the A_0, S_0, and A_1 modes are, respectively, determined by points P_3, P_4, and P_5 in Fig. 2, which are the intersections between the horizontal dash lines (H_3, H_4, H_5) and the $P^*_{zy}(k)$ curve. Considering the fact that the magnitudes of $P^*_{zy}(k_n)$ determined by points P_3 and P_4 are roughly equivalent, it is expected that the same magnitude order of the A_0 and S_0 modes may be generated simultaneously at the frequency $f = 1.15$ MHz. As another example, when the driving frequency f is adjusted to be $f = 0.87$ MHz, only the A_0 and S_0 modes (determined by the intersections between the vertical dashed line V_1 and the Lamb wave dispersion curves in Fig. 2) may be generated. The corresponding magnitudes of $P^*_{zy}(k_n)$ that contribute to the generations of the A_0 and S_0 modes are determined, respectively, by points P_1 and P_2 in Fig. 2, which are the intersections between the horizontal dashed lines (H_1, H_2) and the $P^*_{zy}(k)$ curve. Clearly, the magnitude of $P^*_{zy}(k_n)$ for the generation of the A_0 mode (determined by point P_1) is near the peak of the main lobe and is far larger than that by point P_2. Thus, it is expected that the A_0 mode will play a dominant role and the S_0 mode will be considerably restrained at the frequency $f = 0.87$ MHz.

Based on the previous numerical analyses, the magnitude of $P^*_{zy}(k_n)$ for the generation of the n-th Lamb wave mode can readily be controlled by adjusting the driving frequency (via horizontally moving the vertical dash line like V_1 or V_2 in Fig. 2). The unwanted ultrasonic Lamb wave mode generated by EMAT can be effectively restrained by choosing an appropriate driving frequency.

3.2. Influence of the driving frequency on generations of Lamb wave modes with EMAT

Because the meander-coil EMAT (shown in Fig. 1) can detect only the horizontal displacement component of the ultrasonic wave propagation,[8] the corresponding vertical displacement component is thus no longer considered here. According to Eq. (11), the horizontal displacement component of the n-th Lamb wave mode is given in the following form:

$$U_{nz} = \frac{\pi P^*_{zy}(k_n)}{2P_{nn}}[\hat{z}\cdot\tilde{\boldsymbol{v}}_n(y)]|_{y=+d}[\hat{z}\cdot\boldsymbol{U}_n(y)]\exp(\mathrm{j}k_n z). \quad (12)$$

Based on Eqs. (9)–(11), at several driving frequencies, Tables 1 and 2 show the calculation results of the Lamb wave's mode expansion coefficient and the corresponding horizontal displacement component U_{nz} at the surface ($y = +d$) of the 1.82-mm-thick aluminum sheet, where the Lamb waves are generated by the EMAT with the same geometrical parameters in Fig. 2.

The four driving frequencies (0.87 MHz, 1.15 MHz, 1.85 MHz, and 2.06 MHz) listed in Tables 1 and 2 are given, respectively, by the vertical dash lines V_1, V_2, V_3, and V_4 in Fig. 2. It is deduced from Tables 1 and 2 that the meander-coil EMAT can generate the A_0 and S_0 modes while restraining the generation of the A_1 mode at $f = 1.15$ MHz. Moreover, the magnitude of U_{nz} of the S_0 mode is 1.92 times that of the A_0 mode. When the driving frequency f is set to be 0.87 MHz, the magnitude of U_{nz} of the A_0 mode is 19.7 times that of the S_0 mode. It is expected that the A_0 mode can be effectively generated while the S_0 mode will be considerably restrained. When the driving frequency f is 1.85 MHz, the A_1 mode is the dominant one in these Lamb wave modes generated by the EMAT while the other modes such as S_0, A_0, and S_1 can be largely restrained. Similarly, when the driving frequency f is set to be 2.06 MHz, only the S_1 mode can be generated, while the other modes such as A_0, A_1, S_0, and S_2 will be effectively restrained.

Table 1. Magnitudes of mode expansion coefficient $a_n(z)$ of the n-th Lamb wave generated by EMAT at different frequencies.[a]

Lamb wave modes	A_0	A_1	S_0	S_1	S_2
$f = 1.15$ MHz	0.83	3.04	6.60	–	–
$f = 0.87$ MHz	12.82	–	0.795	–	–
$f = 1.85$ MHz	0.0434	7.70	0.0367	0.117	–
$f = 2.06$ MHz	0.0169	0.427	0.0254	19.8	0.474

[a] The scale of $|a_n(z)|$ is 10^{-13}. The EMAT's geometrical parameters are $a = 0.5$ mm, $D = 3$ mm, $L = 20$ mm, and $g = 0.5$ mm.

Table 2. Magnitudes of the horizontal displacement component U_{nz} (at $y = +d$) of the n-th Lamb wave generated by EMAT at different frequencies[a].

Lamb wave modes	A_0	A_1	S_0	S_1	S_2
$f = 1.15$ MHz	1.44	0.230	2.77	–	–
$f = 0.87$ MHz	4.97	–	0.252	–	–
$f = 1.85$ MHz	0.0938	2.50	0.0584	0.0371	–
$f = 2.06$ MHz	0.0522	0.0217	0.0618	7.07	0.0479

[a] The scale of $|U_{nz}/B_sI|$ is 10^{-13} m^2·N^{-1}. The EMAT's geometrical parameters are $a = 0.5$ mm, $D = 3$ mm, $L = 20$ mm, and $g = 0.5$ mm.

Numerical simulations indicate that the change tendency of the horizontal displacement components of Lamb wave propagation is approximately consistent with that of spatial Fourier transform of the Lorentz surface stress, which is dependent on the EMAT's geometrical parameters. Except for $f = 1.15$ MHz where both the A_0 and S_0 modes can be generated simultaneously, the magnitude of $P^*_{zy}(k_n)$ that contributes to the generation of a single and pure Lamb wave mode is roughly near the peak of the main lobe of the $P^*_{zy}(k)$ curve. Therefore, at a given driving frequency, the relative magnitude of ultrasonic Lamb wave displacement field generated by EMAT can be roughly determined through the $P^*_{zy}(k)$ curve directly.

The above numerical analyses indicate that the driving frequency has an important role in selectively generating or restraining ultrasonic Lamb wave modes when the $P^*_{zy}(k)$ curve of the Lorentz surface stress is given, which is determined by the parameters a, D, and L of the EMAT.[12] That is, the mode expansion coefficient and displacement field of Lamb wave propagation can be appropriately adjusted by choosing the driving frequency of the meander-coil EMAT.

4. Experimental examinations

Some experimental examinations are performed to verify the above theoretical and numerical analyses. The experimental setup for Lamb waves is illustrated in Fig. 3. The Ritec 5000 SNAP system is used to generate tone-burst voltages for the excitation of the meander-coil EMAT *Tx*,[15] and to perform the signal receiving and processing from the receiving EMAT *Rx*. The meander coil of the two EMATs (*Tx* and *Rx*) is fabricated by the printed circuit board (PCB) technique, and its geometrical parameters are $a = 0.5$ mm, $D = 3$ mm, $L = 20$ mm, and $g = 0.5$ mm. The spatial separation Δz between the two EMATs *Tx* and *Rx* is changeable from 180 mm to 280 mm. The elastic sheet used in the experimental examinations is a 1.82-mm-thick aluminum sheet (500 mm×500 mm). For simplicity, the material of the aluminum sheet is assumed to be homogeneous and isotropic. In order to facilitate the experimental observation and signal processing, the duration of the tone-burst excitation voltage is always set to be $\tau = 20$ μs and the magnitude of the receiving signal is enhanced by a 90-dB gain amplifier.

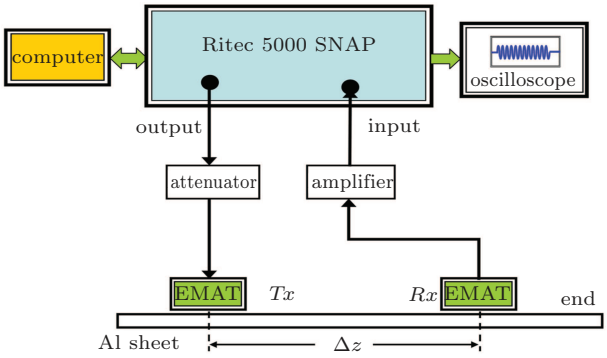


Fig. 3. (color online) Diagram block of experimental setup for ultrasonic Lamb waves generated and detected with meander-coil EMATs.

4.1. Lamb waves generated by EMAT at the frequency $f = 1.15$ MHz

According to the numerical results (shown in Tables 1 and 2), the A_0 and S_0 modes may be generated by the EMAT *Tx* at the driving frequency $f = 1.15$ MHz. The magnitude of U_{nz} of the S_0 mode is slightly larger than that of the A_0 mode (the magnitude of U_{nz} of the S_0 mode is 1.92 times that of the A_0 mode). Figure 4(a) displays the time-domain ultrasonic pulse signal detected by the EMAT *Rx* when the spatial separation Δz between the centers of the two transducers *Tx* and *Rx* is set to be 280 mm.

Clearly, two ultrasonic pulse signals are shown in Fig. 4(a), and the corresponding times of occurrence are around 102 μs and 90 μs, respectively. At the driving frequency $f = 1.15$ MHz, the theoretical group velocities of the A_0, S_0, and A_1 modes are calculated, and their magnitudes are, respectively, 2.890 mm/μs, 3.240 mm/μs, and 4.680 mm/μs. Thus, the theoretical time delays of the A_0, S_0, or A_1 signal should be, respectively, 280/2.89 = 96.9 (μs), 280/3.24 = 86.4 (μs), or 280/4.68 = 59.8 (μs). Therefore, the two ultrasonic pulse signals with time delays of 102 μs and 90 μs (shown in Fig. 4(a)) should correspond to the A_0 and S_0 modes, respectively, where the relative errors of time delay are 5% and 4%, respectively. In order to further identify the ultrasonic Lamb wave modes in the received signal shown in Fig. 4(a), the

corresponding short-time Fourier transform (STFT) spectrogram is calculated and shown in Fig. 4(b), where the straight-through signal from the tone-burst excitation voltage is not taken into account. Figure 4(c) shows the slice at the driving frequency f= 1.15 MHz, through which the magnitudes of the S_0 and A_0 modes can be determined directly. According to Fig. 4(c), the magnitude of the S_0 mode is 1.64 times that of the A_0 mode, which is approximately consistent with the theoretical prediction (the magnitude of U_{nz} of the S_0 mode is 1.92 times that of the A_0 mode).

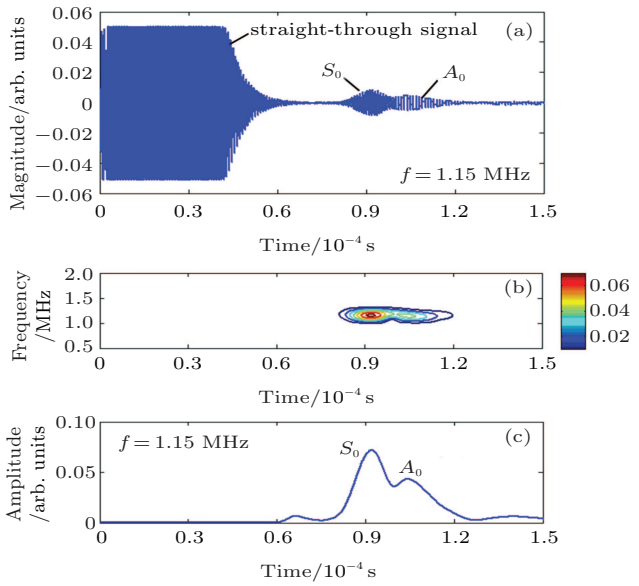


Fig. 4. (color online) Ultrasonic signals at $f = 1.15$ MHz: (a) time–domain signal at $\Delta z = 280$ mm, (b) STFT spectrogram, (c) slice of STFT spectrogram at $f = 1.15$ MHz.

4.2. Lamb waves generated by EMAT at the frequency $f = 0.87$ MHz

Based on the calculation data shown in Tables 1 and 2, the EMAT *Tx* may generate the A_0 mode and restrain the S_0 mode at the driving frequency $f = 0.87$ MHz. To identify the ultrasonic pulse signal received by *Rx*, the values of spatial separation Δz between the EMATs *Tx* and *Rx* are set to be $\Delta z_1 = 280$ mm and $\Delta z_2 = 180$ mm (the position of *Rx* is always kept unchanged), and the corresponding time–domain ultrasonic signals detected from the EMAT *Rx* are displayed in Figs. 5(a) and 5(b) (horizontal scale: 20 μs/div), respectively.

Clearly, if the reflected signal induced by the end of the Al sheet is not taken into account, only one ultrasonic pulse signal can be observed. The time widths of the square window (yellow) in Figs. 5(a) and 5(b) are set to be the same, i.e., $t = 35$ μs. The group velocity of the ultrasonic pulse signal in Fig. 5 is calculated by $(\Delta z_1 - \Delta z_2)/t$, and its magnitude is around 2.857 mm/μs. The theoretical group velocities of the A_0 and S_0 modes at the driving frequency $f = 0.87$ MHz are calculated to be 2.760 mm/μs and 4.770 mm/μs, respectively. Therefore, the ultrasonic pulse signal in Fig. 5 should correspond to the A_0 mode (the relative error of group velocity is around 3.5%). Similarly, to further identify the ultrasonic Lamb wave mode, the corresponding STFT spectrogram of the ultrasonic pulse signal at $\Delta z_1 = 280$ mm (shown in Fig. 6(a)) is calculated and shown in Fig. 6(b). Figure 6(c) shows the slice at the driving frequency $f = 0.87$ MHz. Through the above analyses, when the driving frequency f is set to be 0.87 MHz, the EMAT can generate only the A_0 mode and restrain the generation of the S_0 mode effectively.

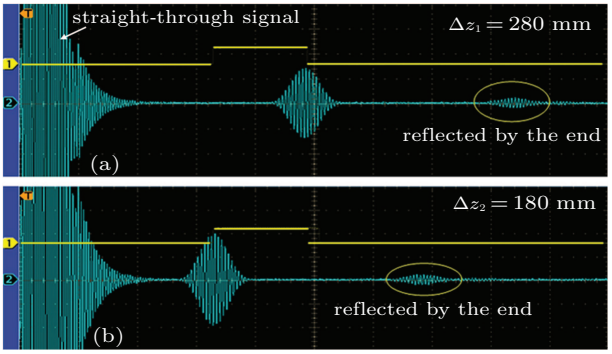


Fig. 5. (color online) Ultrasonic pulse signals at $f = 0.87$ MHz, (a) $\Delta z_1 = 280$ mm, (b) $\Delta z_2 = 180$ mm.

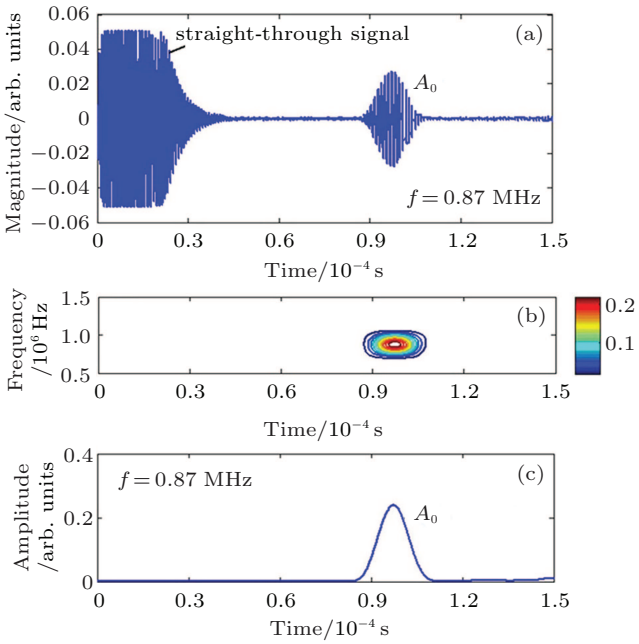


Fig. 6. (color online) Ultrasonic signals at $f = 0.87$ MHz: (a) time–domain signal at $\Delta z = 280$ mm, (b) STFT spectrogram, (c) slice of STFT spectrogram at $f = 0.87$ MHz.

4.3. Lamb waves generated by EMAT at the frequency $f = 1.85$ MHz

According to the numerical results (shown in Tables 1 and 2), when the driving frequency is set to be 1.85 MHz, the EMAT may generate only the A_1 mode and restrain the other modes. Similarly, the values of the spatial separation between the two EMATs *Tx* and *Rx* are set to be $\Delta z_1 = 280$ mm and $\Delta z_2 = 180$ mm, and the corresponding time–domain ultrasonic

signals detected from the EMAT *Rx* are displayed in Figs. 7(a) and 7(b), respectively.

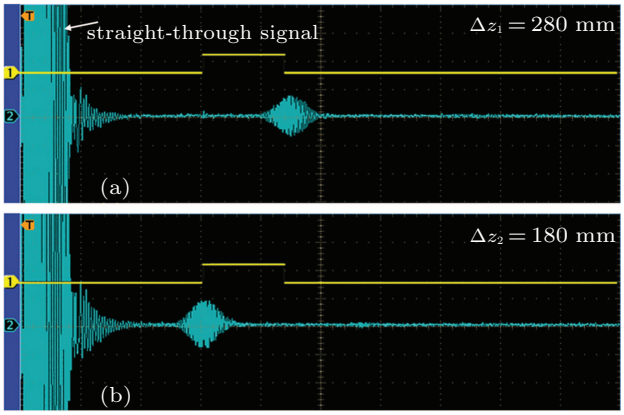


Fig. 7. (color online) Ultrasonic pulse signals at $f = 1.85$ MHz: (a) $\Delta z_1 = 280$ mm, (b) $\Delta z_2 = 180$ mm.

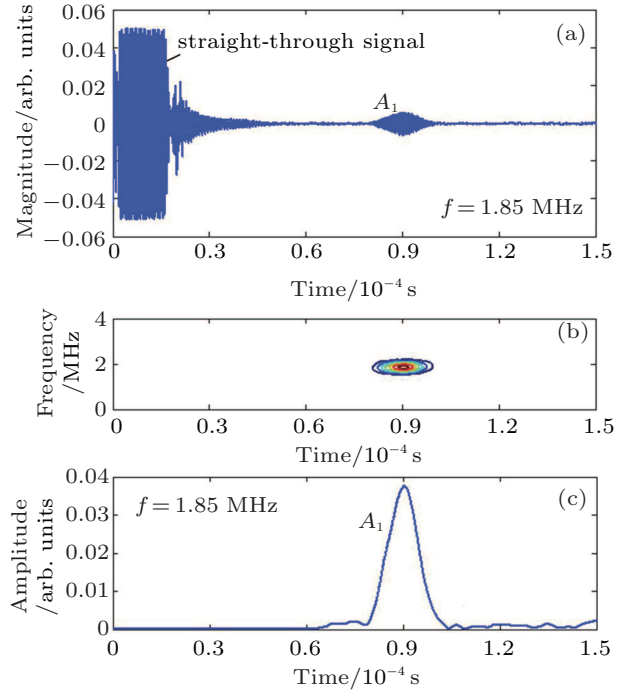


Fig. 8. (color online) Ultrasonic signals at $f = 1.85$ MHz: (a) time–domain signal at $\Delta z = 280$ mm, (b) STFT spectrogram, (c) slice of STFT spectrogram at $f = 1.85$ MHz.

Clearly only one ultrasonic pulse signal can be observed. The time widths of the square window (yellow) in Figs. 7(a) and 7(b) are set to be the same, i.e., $t = 26$ μs. The group velocity of the ultrasonic pulse signal in Fig. 7 is calculated from $(\Delta z_1 - \Delta z_2)/t$, and its magnitude is around 3.85 mm/μs, which is very close to the theoretical group velocity of the A_1 mode (3.71 mm/μs) in all Lamb wave modes generated by EMAT at the driving frequency $f = 1.85$ MHz (the relative error of group velocity is 3.6%). Similarly, figures 8(b) and 8(c) are, respectively, the STFT spectrogram and the corresponding slice at the driving frequency $f = 1.85$ MHz of the ultrasonic pulse signal at $\Delta z_1 = 280$ mm (shown in Fig. 8(a)). Through the above experimental examination, when the driving frequency f is set to be 1.85 MHz, only the A_1 mode can be generated while the other modes such as S_0, A_0, and S_1 are restrained effectively.

4.4. Lamb waves generated by EMAT at the frequency $f = 2.06$ MHz

The calculation data listed in Tables 1 and 2 indicate that the EMAT *Tx* can generate only the S_1 mode while restraining the generations of the other modes at the driving frequency $f = 2.06$ MHz. When the values of spatial separation between the EMATs *Tx* and *Rx* are set to be $\Delta z_1 = 280$ mm and $\Delta z_2 = 180$ mm, the corresponding time-domain ultrasonic pulse signal detected from the EMAT *Rx* is displayed in Fig. 9.

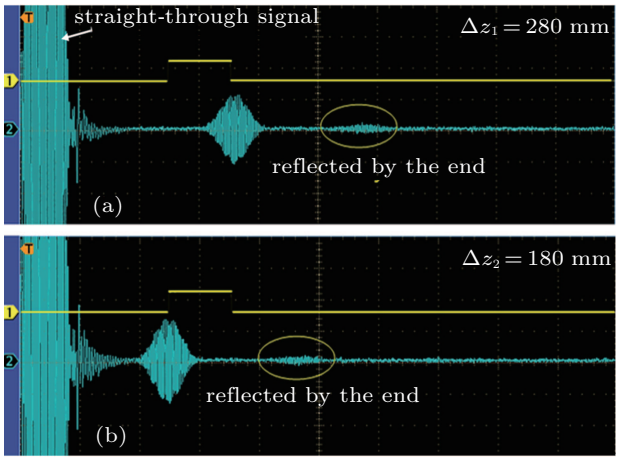


Fig. 9. (color online) Ultrasonic pulse signals at $f = 2.06$ MHz: (a) $\Delta z_1 = 280$ mm, (b) $\Delta z_2 = 180$ mm.

Clearly, if the reflected signal induced by the end of the Al sheet is not taken into account, only one ultrasonic pulse signal can be observed in Fig. 9. The time widths of the square window (yellow) in Figs. 9(a) and 9(b) are set to be the same, i.e., $t = 20$ μs. The group velocity of the ultrasonic pulse signal in Fig. 9 is calculated from $(\Delta z_1 - \Delta z_2)/t$, and its magnitude is around 5.00 mm/μs, which is very close to the theoretical group velocity of the S_1 mode (4.75 mm/μs) in all Lamb wave modes generated by EMAT at the driving frequency $f = 2.06$ MHz (the error of group velocity is round 5.5%). Similarly, figures 10(b) and 10(c) are, respectively, the STFT spectrogram and the corresponding slice at the driving frequency $f = 2.06$ MHz of the ultrasonic pulse signal at $\Delta z_1 = 280$ mm (shown in Fig. 10(a)). It is obvious that when the driving frequency f is set to be 2.06 MHz, only the S_1 mode can be generated, and the other modes such as A_0, A_1, S_0, and S_2 are restrained effectively.

Through the above experimental examinations that are consistent with the theoretical predictions, it is experimentally verified that ultrasonic Lamb wave modes generated by EMAT

can be effectively regulated (strengthened or restrained) by choosing an appropriate driving frequency when the EMAT's geometrical parameters a, D, and L are given.

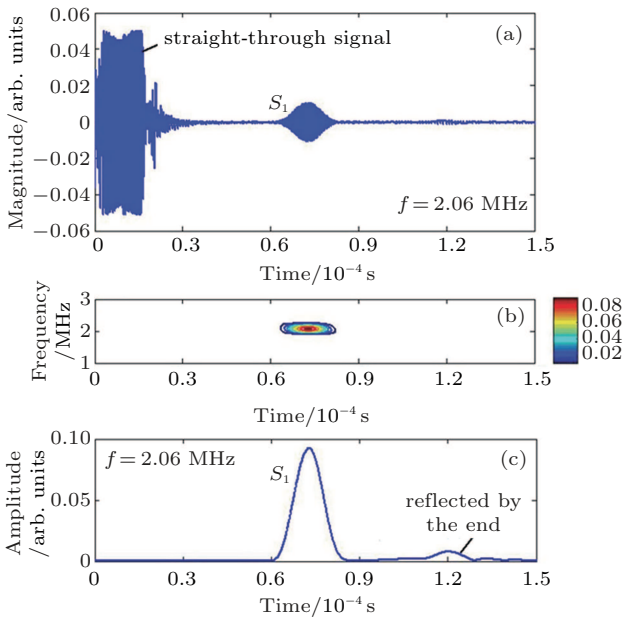


Fig. 10. (color online) Ultrasonic signals at $f = 2.06$ MHz: (a) time–domain signal at $\Delta z = 280$ mm, (b) STFT spectrogram, (c) slice of STFT spectrogram at $f = 2.06$ MHz.

5. Conclusions

As described above, a modal expansion approach is proposed for investigating the generations of the ultrasonic Lamb waves with a meander-coil EMAT. The formal solution for the Lorentz surface stress exerted on the surface of a non-ferromagnetic sheet is derived, and then the spatial Fourier transform on the Lorentz surface stress that contributes to the generations of the ultrasonic Lamb waves is obtained. On this basis, with the modal expansion approach for waveguide excitation, the analytical expression of the Lamb wave's mode expansion coefficient is deduced, which is closely related to the driving frequency and the EMAT's geometrical parameters. The obtained analytical expression of the displacement field of the Lamb wave mode lays a theoretical foundation for exactly analyzing the generations of Lamb waves with a meander-coil EMAT. Further, the numerical analyses and experimental examinations indicate that the Lamb wave's mode expansion coefficient and displacement field can be appropriately adjusted by choosing the driving frequency when the EMAT's geometrical parameters are given. This result provides a theoretical and experimental basis for selectively generating a single and pure Lamb wave mode with EMATs.

References

[1] Kim H P, Lee S H and Kim Y Y 2013 *Journal of Sound and Vibration* **332** 740
[2] Zhou D, Liu X Z, Gong X F, Nazarov V E and Ma L 2009 *Chin. Phys. B* **18** 898
[3] Hao K S, Huang S L, Zhao W, and Wang S 2011 *Chin. Phys. B* **20** 068104
[4] Zhang H Y and Yu J B 2011 *Chin. Phys. B* **20** 094301
[5] Deng M X and Xiang Y X 2010 *Chin. Phys. B* **19** 114302
[6] Xiang Y X and Deng M X 2008 *Chin. Phys. B* **17** 4232
[7] Dhayalan R and Balasubramaniam K 2010 *NDT & E International* **43** 519
[8] Masahiko H and Hirotsugu O 2003 *EMATs for Science and Industry on-contacting Ultrasonic Measurements* (Boston: Kluwer Academic publishers)
[9] Rueter D and Morgenstern T 2014 *Ultrasonics* **54** 2141
[10] Zhai G, Jiang T and Kang L 2014 *Ultrasonics* **54** 632
[11] Hirao M and Ogi H 1997 *Ultrasonics* **5** 413
[12] Li M L, Deng M X and Gao G J 2014 *Chinese Journal of Acoustics* **33** 156
[13] Ismael N, Ros K I and Carlos N 2000 *J. Acoust. Soc. Am.* **107** 2370
[14] Auld B A 1973 *Acoustic Fields and Waves in Solids* (New York: Wiley)
[15] Ritec Advanced Measurement System 2000 Model SNAP-0.25-7 *Operation Manual RITEC* (USA)